Improved Ring-Based Photonic Crystal Raman Amplifier Using Optofluidic Materials

Amire Seyedfaraji

Abstract Ring-based photonic crystal (PhC) structure for Raman amplifier is investigating in this article. Then using optofluidic materials in the holes on the sides of the signal path, pump and signal group velocity reducing that cause Raman gain increase. In order to achieve bigger Raman gain, we use two-ring structure. The time evolution and propagation of picosecond signal pulses and dispersion inside the device are analyzed and Raman gain, Raman bandwidth and bit rate are studied in one-ring and two-ring structures. Maxwell equations are solved by finite difference time domain (FDTD) method and considering the optical nonlinear parameters of two photon absorption, free carrier absorption, Kerr effect and self-phase modulation in PhC structure. From a structure with a length of 100 μm, Raman gain of 19.01 dB and bit rate of 0.6493×10^{12} pulse/sec are achieved.

Keywords Raman amplifier · Ring-based · Photonic crystal · Optofluidic materials · Bit rate · Maxwell equation

1 Introduction

Recently, we observe a significant development in use of silicon (Si) based fast modulators, photo-detectors, optical amplifiers and sources. Silicon photonics is turning out as low-cost optoelectronic solutions for a variety of applications from telecommunications and interconnects to optical sensing and biomedical applications. Stimulated Raman scattering has been used as a successful approach for optical amplification and lasing in Si [1].

In Raman spontaneous scattering, thermal vibration of lattice at frequency ω_v, produce a sinusoidal modulation in optical susceptibility. This frequency is 15.6 THz in Si. With a collision of input pump field (ω_l), with optical susceptibility

A. Seyedfaraji (✉)
Faculty of Engineering and Technology, Alzahra University,
P.O. Box 1993893973, Tehran, Iran
e-mail: sfaraji@alzahra.ac.ir

(ω_v), some polarizations create at the sum frequency ($\omega_v + \omega_l$), and at the difference frequency ($\omega_l - \omega_v$). The radiation produced by these two polarization components, respectively called anti-Stokes and Stokes waves. In stimulated Raman scattering, atomic vibration can be excited by simultaneous propagation of pump and Stokes field, which amplifies the Stokes field [2].

In recent years, Raman gain in Si waveguides has been extensively studied [3–5]. For improve the efficiency of Raman amplifiers, Si nano waveguides [6], SiGe waveguides [7], PhC [8, 9], and hybrid PhC (HPhC) waveguides [10] and slow-light grating waveguides [11] have been used. Some rules have been developed to design Raman amplifiers, using analytical and semi-analytical methods [12] and geometric waveguides parameters have been optimized to improve Raman amplifiers performance [13].

On the other hand, in slow-light regime, where light moves slower through the material, light-matter interaction time is increased and nonlinear effects will be intensified. As well as reduction of group velocity reduces the pump power or physical length required to appear nonlinear effects. For this reason, to reduce the size and increase the intensity of nonlinear effects, slow light is employed [14, 15].

PhC waveguides, provide strong mode confinement and low-group velocities through structural Bragg reflections. Such properties account for enhancing nonlinear optical phenomena such as Raman scattering and therefore larger Raman gain will be obtained with smaller input pump power [16].

To make efficient use of the pump power, we have already presented a new configuration of ring-based Raman amplifier [17], PhC ring-based Raman amplifier and HPhC ring-based Raman amplifier [18]. The resonance effect enhances the effective pump power and thus can achieve the same level of Raman gain at a much lower input pump power.

In this paper, using optofluidic materials [19, 20] in the holes on the sides of the signal path, we reduce the group velocity for signal and pump wavelength and increase the matter and light interaction time which consequently results in stronger nonlinear effects. In this way, by decreasing group velocity in PhC ring-based structure, input pump power can be reduced and higher Raman gain can be achieved.

This paper is organized as follows. In Chap. 2 Using Maxwell equations, we model Raman amplification in PhC waveguides considering nonlinear effects of two photonic absorption (TPA), free carrier absorption (FCA), Kerr effect and self-phase modulation (SPM) effect. Chap. 3 deals with Raman amplification simulation results in PhC ring-based structure and improved PhC ring-based structure. We summarize the results of the paper in Chap. 4.

2 Modeling Theory

As a consequence of Kerr nonlinear effect, two photon absorption effect and other nonlinear effects, the refractive index of a material is dependent on the optical power. When a strong light pulse passes through a medium, it will induce a phase

shift $\Delta\varphi$ due to optical nonlinearities. When ultra short pulses are used, the intensity rapidly varies in time which results in phase change. The time derivative of the phase change yields a frequency shift $\Delta\omega$ across the pulse defined by (1)

$$\Delta\omega(x, y, t) = -\frac{d(\Delta\varphi(x, y, t))}{dt} \qquad (1)$$

That $\Delta\varphi$ is given by (2) [21].

$$\Delta\varphi(x, y, t) = \frac{2\pi L_{\text{int}}}{\lambda_P}(\Delta n_{kerr}(x, y, t) + \Delta n_{FC}(x, y, t)) \qquad (2)$$

L_{int} is the interaction length. Δn_{kerr} is Kerr-induced refractive index change and Δn_{FC} is free-carrier induced refractive index change. λ_p is center wavelength of the pump pulse along the waveguide.

As a result of falling and rising edges of $\Delta\varphi$, positive and negative changes create in $\Delta\omega$. In addition, passing the pump pulse from anywhere on the waveguide, causes carrier density to be increased, which consequently results in larger reflective index. So, central wavelength will have blue shift. Center wavelength of the pump pulse is given by (3) in each point [21].

$$\lambda_P(x, y, t) = \frac{\lambda_0}{1 - (L_{\text{int}}/c).(d\Delta n(x, y, t)/dt)} \qquad (3)$$

In this equation, Δn is the sum of the changes of reflective index arises from nonlinear Kerr effect and FCA effect. λ_0 is initial wavelength of entrance pump pulse, and c is light velocity.

By increasing pump power, the losses due to TPA and FCA are intensified. So these two phenomena should be considered in simulation [22]. Raman effect and TPA are modeled with 3rd order nonlinear optical susceptibility [23, 24]. TPA causes some carrier density changes that affect the refractive index and gain coefficient and therefore real and imaginary parts of the first order optical susceptibility are changed [24]. SPM effect is modeled with real part of 3rd order nonlinear optical susceptibility. Considering these effects, the electric polarization for the pump and signal are given by (4) and (5).

$$\begin{aligned} \mathbf{P_S} &= \mathbf{P}(\omega_S) \\ &= \chi(\omega_S)\mathbf{E_S} + \varepsilon_0\chi_{\text{Im}}^{(3)}(\omega_S)\mathbf{E_P}.\mathbf{E_P^*}.\mathbf{E_S} + \varepsilon_0\chi_{\text{Im}}^{(3)}(\omega_S)\mathbf{E_S}.\mathbf{E_S^*}.\mathbf{E_S} + \varepsilon_0\chi_P^{(f)}(\omega_S, N)\mathbf{E_S} \end{aligned} \qquad (4)$$

$$\begin{aligned} \mathbf{P_P} &= \mathbf{P}(\omega_P) = \chi(\omega_P)\mathbf{E_P} + \varepsilon_0\chi_{\text{Im}}^{(3)}(\omega_P)\mathbf{E_S}.\mathbf{E_S^*}.\mathbf{E_P} + \varepsilon_0\chi_{\text{Im}}^{(3)}(\omega_P)\mathbf{E_P}.\mathbf{E_P^*}.\mathbf{E_P} \\ &\quad + \varepsilon_0\chi_P^{(f)}(\omega_P, N)\mathbf{E_P} + \varepsilon_0\chi_{\text{Re}}^{(3)}(\omega_P)\mathbf{E_P}.\mathbf{E_P^*}.\mathbf{E_P} \end{aligned} \qquad (5)$$

where $\mathbf{E_s}$ is signal electric field, $\mathbf{E_p}$ is pump electric field, ε_0 is permittivity of free space. N is carrier density. ω_S and ω_P are signal and pump frequency, respectively. χ is the first order optical susceptibility and $\chi_{\mathrm{Im}}^{(3)}$ and $\chi_{\mathrm{Re}}^{(3)}$ are imaginary part and real part of 3rd order nonlinear optical susceptibility, respectively. $\chi^{(f)}$ is the optical susceptibility that models the FCA defined as (6) [24].

$$\chi_v^{(f)} = 2n_0 \left(n_{fv} + ic\frac{\alpha_{fv}}{2\omega_v} \right) \tag{6}$$

$$n_{fv}(\omega_v, N) = -\frac{q^2 N}{2\varepsilon_0 n_0 \omega_v^2} \left(\frac{1}{m_{ce}} + \frac{1}{m_{ch}} \right) \tag{7}$$

$$\alpha_{fv}(\omega_v, N) = \frac{q^3 N}{\varepsilon_0 c n_0 \omega_v^2} \left(\frac{1}{\mu_e m_{ce}^2} + \frac{1}{\mu_h m_{ch}^2} \right) \tag{8}$$

where the index v denotes S or P for signal or pump, respectively. n_0 is linear refractive index, n_{fv} is free carrier index change or rate of change in the refractive index due to the carrier density changes and α_{fv} is free carrier absorption or rate of change in the absorption coefficient due to the carrier density changes. m_{ce}, m_{ch}, μ_e and μ_h are effective mass of electron, effective mass of hole, electron mobility and hole mobility, respectively [24].

Carrier density change caused by TPA is modeled as (9)

$$\frac{dN}{dt} = -\frac{N}{\tau} + \frac{\beta_2(\omega_S)I_S^2}{2\hbar\omega_S} + \frac{\beta_2(\omega_P)I_P^2}{2\hbar\omega_P} \tag{9}$$

$$I_S = \frac{\varepsilon_0 cn}{2}|E_S|^2 \quad I_P = \frac{\varepsilon_0 cn}{2}|E_P|^2 \tag{10}$$

$$\beta_2(\omega) = \frac{3\omega\chi_{\mathrm{Im}}^{(3)}}{2\varepsilon_0 c^2 n_0^2} \tag{11}$$

where β_2 is TPA coefficient and τ is the carrier lifetime.

The Kerr effect causes the linear refractive index of a material to be linearly dependent on the optical intensity, according to (12)

$$n = n_0 + n_2 I_P \tag{12}$$

where n_2 is Kerr coefficient [21].

We obtain the relative permittivity from electric polarization and substitute it into Maxwell's equations and solve them using the finite difference time domain (FDTD) method. A perfectly matched layer boundary condition has been used.

3 Results and Discussion

Schematic structure of proposed PhC ring-based Raman amplifier (SR) and improved PhC ring-based Raman amplifier using optofluidic materials (SR-a) are shown in Fig. 1a, b, respectively.

These micro rings have been made in Si hexagonal 2D PhC slab with air holes. Structure period is a and holes radii are r. Structural parameters should be selected
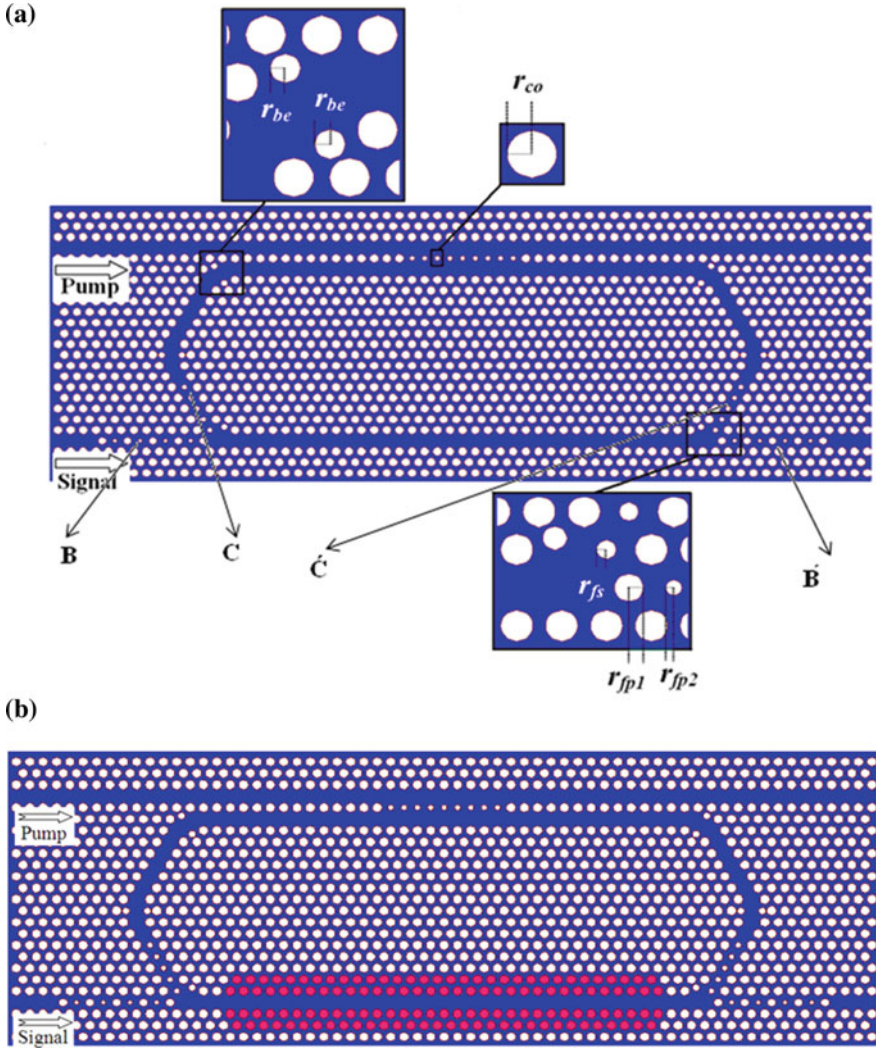

Fig. 1 Structure of **a** PhC ring-based Raman amplifier (SR), and **b** improved PhC ring-based Raman amplifier using optofluidic materials (SR_a)

such that pump wavelength (TM, 1.55 µm) and signal wavelength (TE, 1.686 µm) propagate inside the PhC waveguide.

These structures have two separate entrances for pump and signal [18]. Upper waveguide is the entrance of pump. The perimeter of the ring is optimized for the resonance of pump wavelength. The geometric parameters have been selected such that the structures have critical coupling for pump wavelength. Lower waveguide is the entrance of signal which passes through the lower side of the ring.

Inside the waveguide before the ring and after that indicated by B and B′, several air holes (nano defects) with specified radii and distances are designed such that pump wavelength cannot pass. We call these two parts as pump filter. Thus pump wavelength can resonate inside the ring causing its intensity to be increased. On the other hand, inside the two sides of the ring that indicated by C and C′, air holes (nano defects) with specified radii and distances that are called signal filter prevent the signal entry. So, the signal only passes the direct path without any perturbation inside the ring.

In Fig. 1b using optofluidic materials in the holes on the sides of the signal path, the advantage of lower group velocity can be used more efficiently. The refractive index of optofluidic material is n_{of}.

Geometric properties of these structures are presented in Table 1.

Transmission spectra of pump and signal filter, corresponding to B, B′ and C, C′, are shown, respectively in Figs. 2 and 3. In these figures, part (a) corresponds to around pump wavelength (TM, 1.55 µm) and part (b) is relevant to the signal wavelength (TE, 1.686 µm). As can be seen, pump filter does not pass pump wavelength and signal filter does not pass signal wavelength, whereas pump wavelength and signal wavelength pass respectively through the signal filter and pump filter with very little loss.

There are different methods to improve the quality of passing through the bend in PhC structures [19, 20, 25, and 26]. Due to the [25] to design the bends, the air hole at the inner corner is made smaller, and one air hole is added at the outer corner of the bend. The two air holes have the radii of $r_{be} = 0.75 \times r$, and they are moved $0.3 \times a$ oppositely along the symmetric axis of the bend.

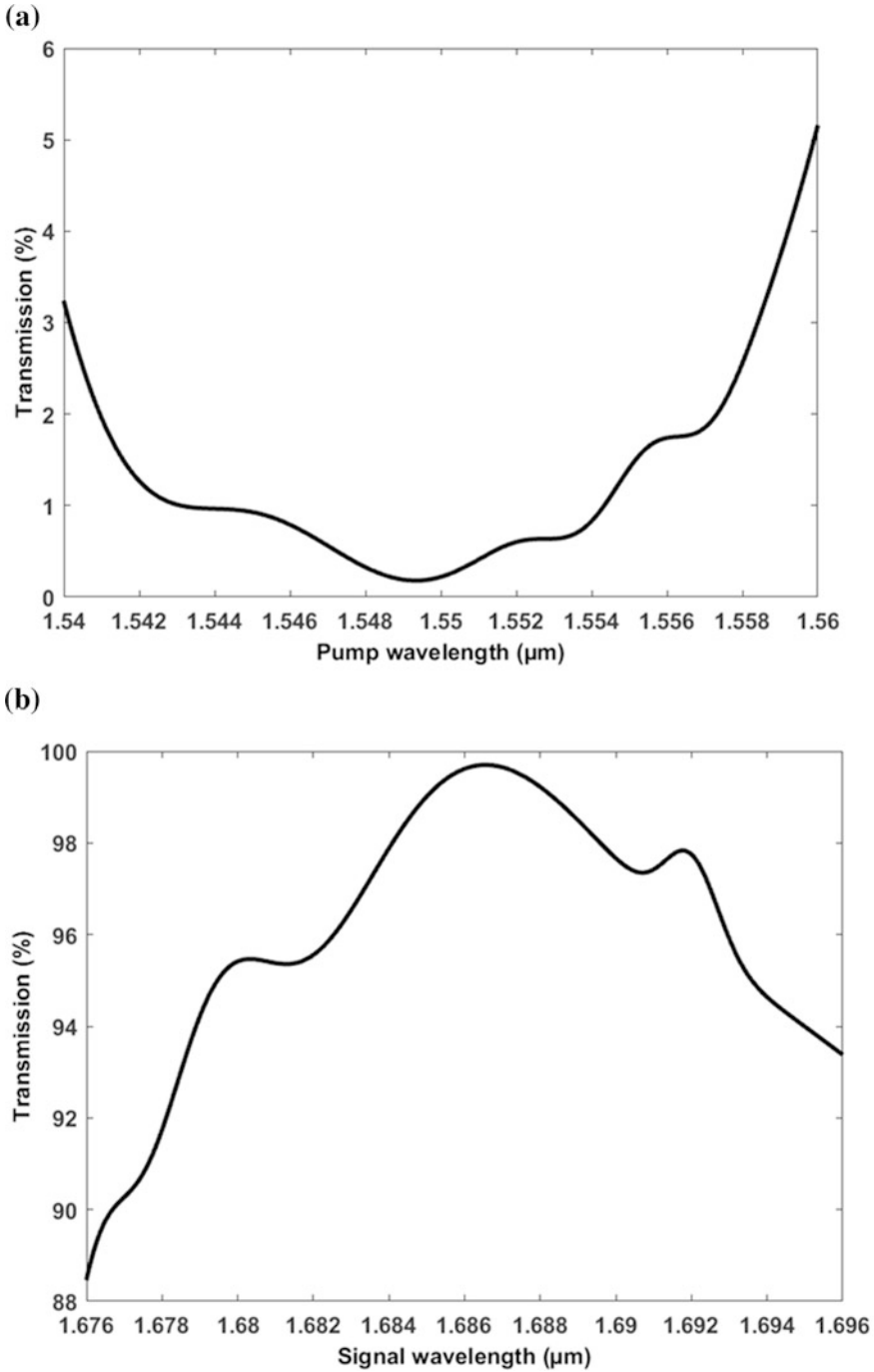| Table 1 Physical parameters of PhC ring-based Raman amplifiers		SR	SR_a
	a (nm)	460	460
	r (nm)	165.6	165.6
	r_{fs}(nm)	89.7	89.7
	r_{fp1}(nm)	147.2	147.2
	r_{fp2}(nm)	69	69
	r_{co}(nm)	308.2	308.2
	r_{be}(nm)	124.2	124.2
	n_{of}	–	1.5

(a)

(b)

Fig. 2 Transmission spectra of pump filter around **a** pump wavelength and **b** signal wavelength
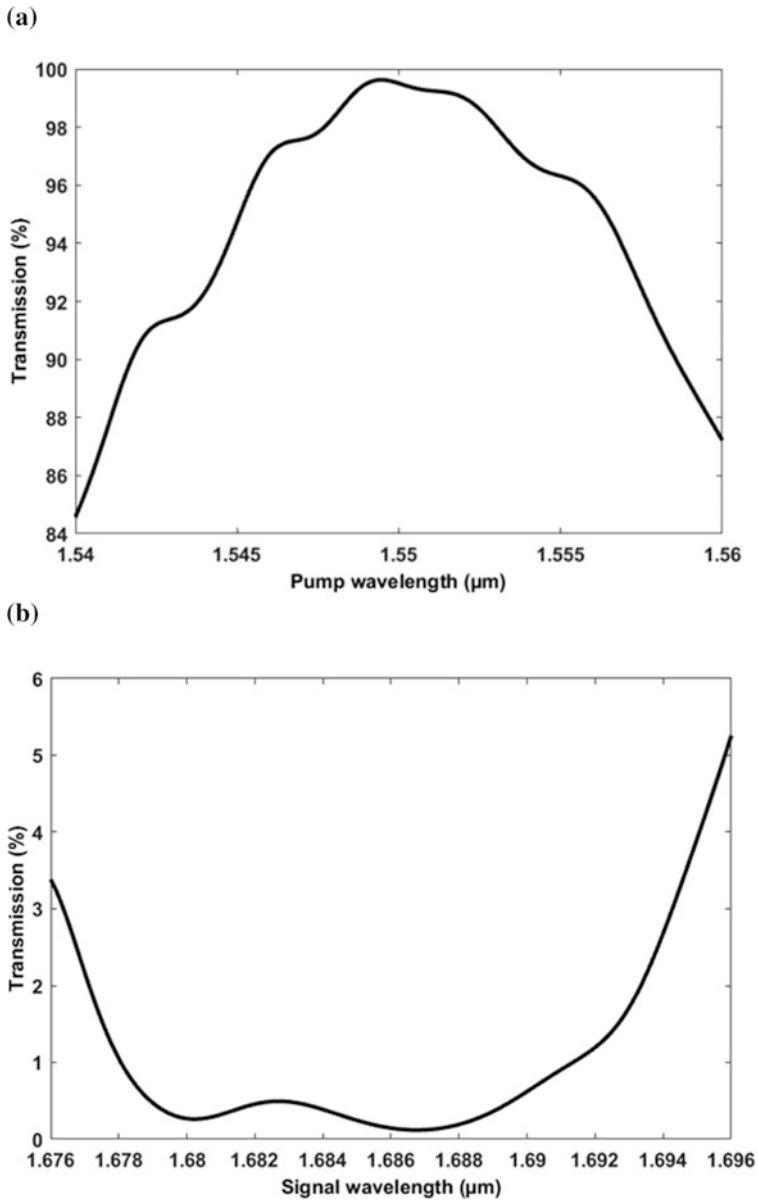
(a)

(b)

Fig. 3 Transmission spectra of signal filter around **a** pump wavelength and **b** signal wavelength

The bend transmission spectra around pump wavelength (TM, 1.55 μm) of PhC ring-based structure is shown in Fig. 4. As can be seen, pump wavelength pass through the bend with little loss.
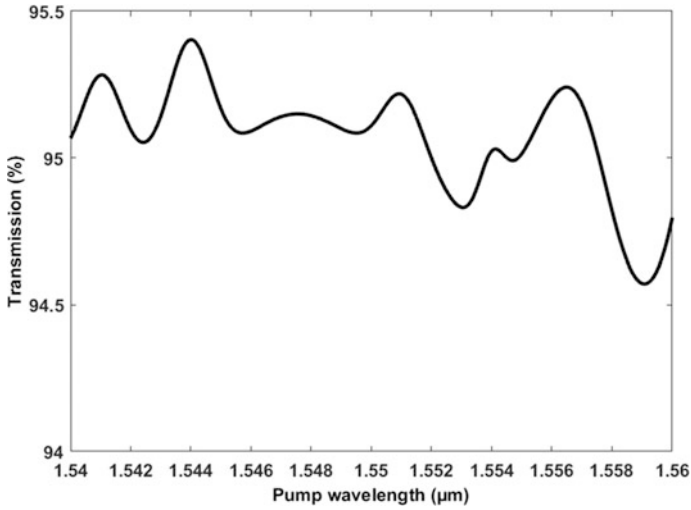
Fig. 4 The bend transmission spectra around pump wavelength (TM, 1.55 μm) of PhC ring-based structure
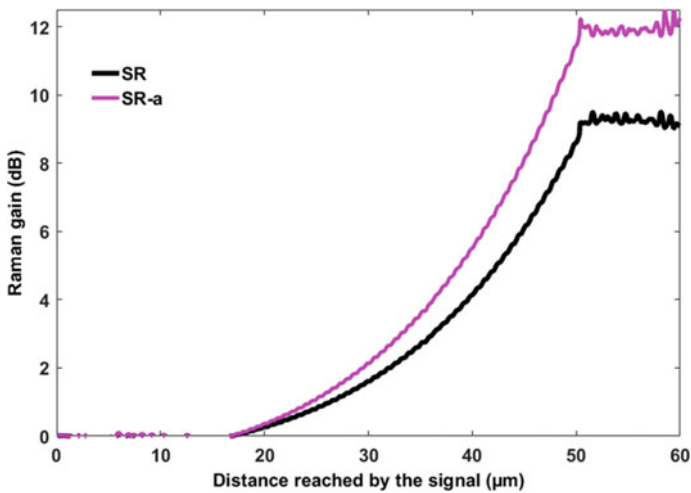

Fig. 5 Raman gain along signal path for 2 ring-based PhC structures (SR and SR-a) for pump power of 0.3 W

Figure 5 shows Raman gain along signal path for these 2 structures (SR and SR-a). Length of amplification region in these structures is about 35 μm and pump power is 0.3 W. Each of these curves has three parts. The first and the last parts correspond to regions where the signal passes through them but the pump is prevented to enter. Thus, no additional Raman gain is created. There is small amount

of noise caused by structural scattering. The middle part is relevant to the region where both signal and pump are simultaneously present which results in Raman gain.

By filling the holes on the two sides of the signal path by optofluidic materials (SR-a), pump and signal group velocity are reduced causing a higher Raman gain compared with SR structure. So that, Raman gain in the output of SR-a structure is almost 3 dB greater than obtained Raman gain of SR structure.

To achieve greater Raman gain we can add an extra ring along the first one, as shown in Fig. 6. Here we assume that these two rings have no coupling with each other.

Figure 7 shows Raman gain along signal path for two-ring Raman amplifiers (SR and SR_a). Pump power is 0.3 W. As shown in this figure, for a specified
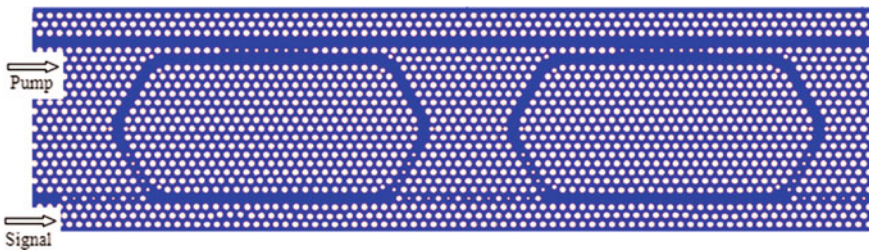

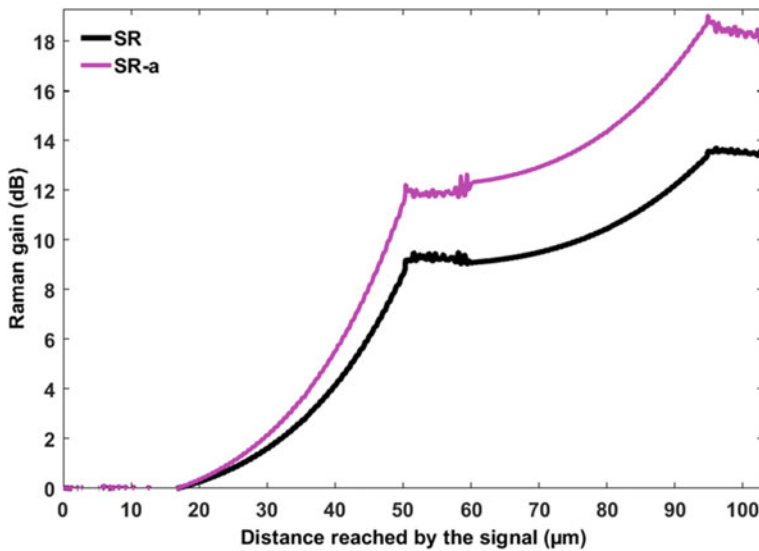**Fig. 6** Two ring-based PhC Raman amplifier structure

Fig. 7 Raman gain along signal path for two-ring Raman amplifiers (SR and SR-a). Pump power is 0.3 W

amount of input pump power, Raman gain has almost doubled compared to the single ring structures. As well as using optofluidic materials in SR-a structure has caused Raman gain to be about 6 dB greater than Raman gain in SR structure for input pump power of 0.3 W.

High Raman gain is one of the important parameters in choosing the structure of Raman amplifier. Another important parameter for evaluation of Raman amplifier's performance is bit rate of input pulses which corresponds to the minimum time distance between successive pulses. As the input pulse passes through the waveguide and both the initial and final parts (pump filters) creates dispersion and therefore signal pulse is broadened in time domain. Thus the minimum distance between successive pulses increases and bit rate is reduced.

Figures 8 and 9 show the time evolutions of output signal for, respectively, single-ring and 2-ring PhC-based Raman amplifier structures (SR and SR-a) for propagation of 3 successive pulses.
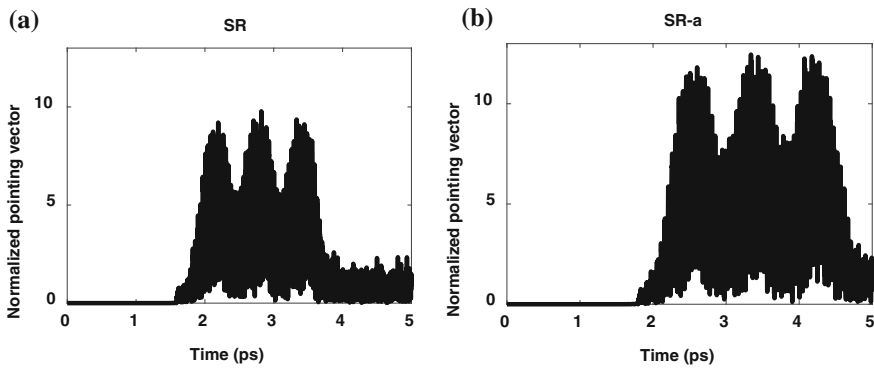

Fig. 8 Single-ring PhC-based amplifiers output after sending three successive signal pulses. Pump power is 0.3 W
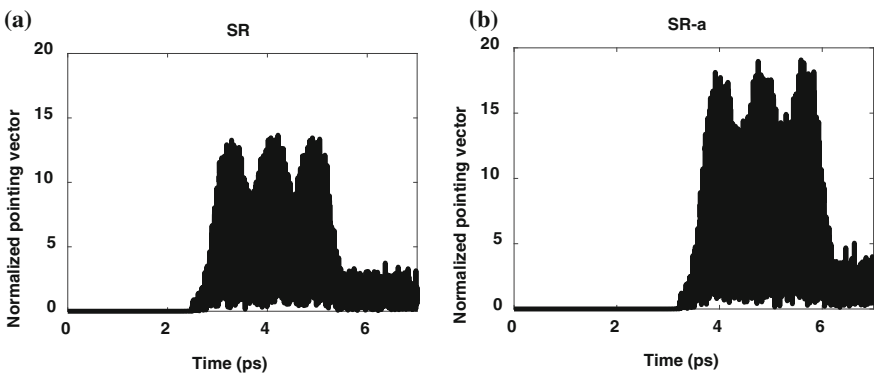

Fig. 9 2-ring PhC-based amplifiers output after sending three successive signal pulses. Pump power is 0.3 W
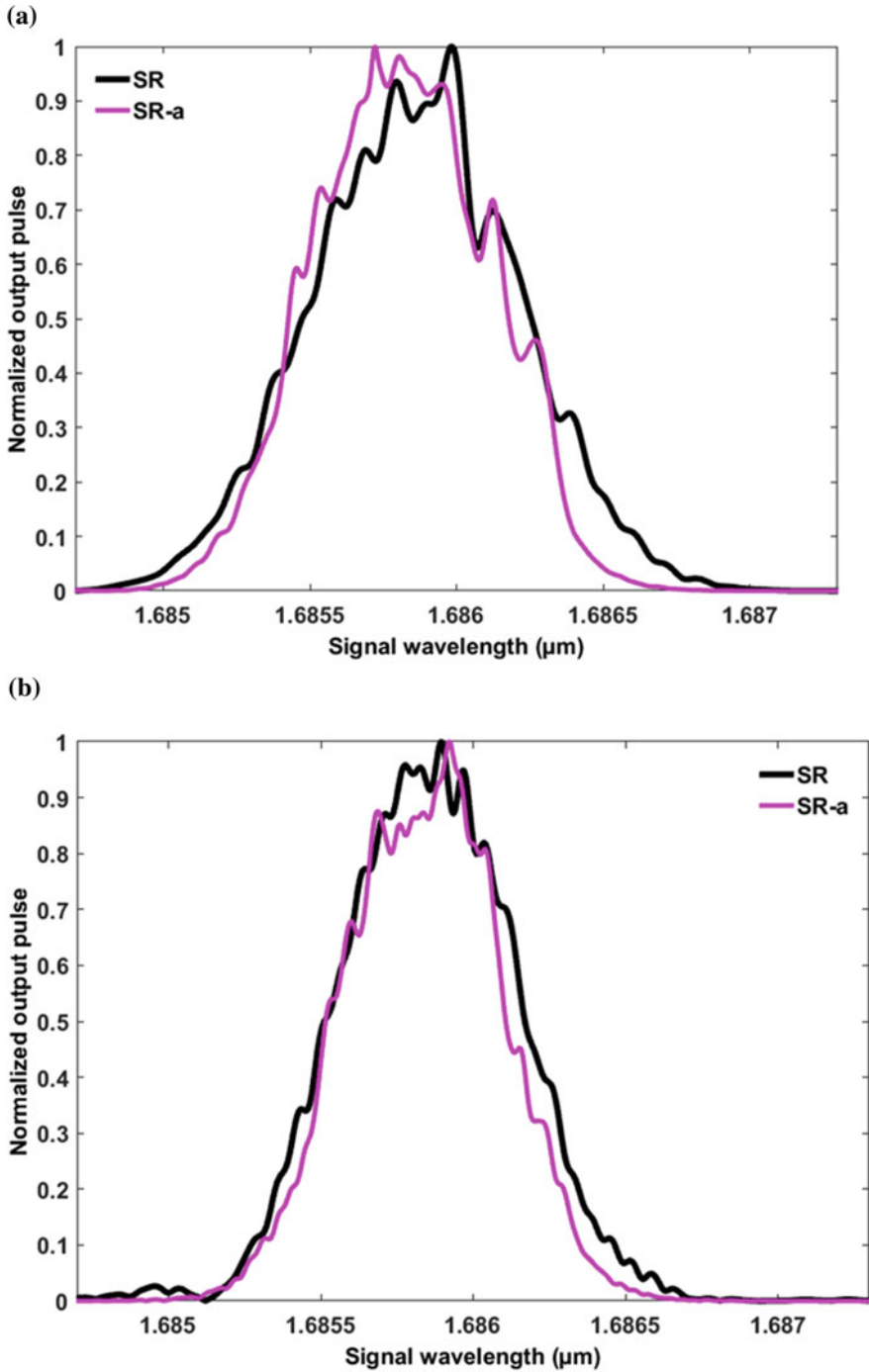
(a)

(b)

Fig. 10 Fourier transform of signal output pulses for **a** single-ring and **b** 2-ring PhC-based Raman amplifiers. Pump power is 0.3 W

Table 2 Results of Raman gain, bit rate and FWHM study in SR and SR-a Raman amplifiers

	SR (single-ring)	SR-a (single-ring)	SR (2-ring)	SR-a (2-ring)
Raman Gain(dB)	9.192	12.19	13.56	19.01
Bit rate ($\times 10^{12}$ s)	0.759	0.716	0.7077	0.6493
FWHM (nm)	0.79	0.77	0.69	0.64

The pump power is 0.3 W

Comparing the results of Figs. 8 and 9, we find that the short length path traveled by the signal in single-ring based structures provides smaller dispersion in the output. However, in two-ring Raman amplifiers, longer signal path gives larger Raman gain. On the other hand, using optofluidic materials in SR_a structure increases Raman gain significantly, but increases dispersion a little. Therefore, SR_a has a proper bit rate besides having great Raman gain.

For better understanding of the dispersion effect on the output signal pulses, Fourier transform of output pulses are shown in Fig. 10a, b for single-ring and 2-ring PhC-based Raman amplifiers, respectively. The results exhibit that dispersion reduces the pulse width in frequency domain. In single-ring structures the dispersion's full width at half maximum (FWHM) is larger than two-ring structure.

For better comparison, the obtained values of Raman gain, bit rate and FWHM of single-ring and two-ring SR and SR_a structures are summarized in Table 2. As can be seen, single-ring SR structure exhibits the lowest Raman gain and the largest bit rate (the lowest dispersion). In two-ring Raman amplifiers, longer signal path gives larger Raman gain and greater dispersion. The greatest Raman gain and smallest bit rate is seen in two-ring SR-a structure.

4   Conclusion

PhC ring-based Raman amplifier (SR) and improved PhC ring-based Raman amplifier (SR_a) have been compared in this paper. Using optofluidic materials in the holes on the sides of the signal path in the improved PhC structure (SR-a) has caused enhancement in Raman gain significantly, with same input pump power. So that, the obtained Raman gain from SR-a structure is about 2.99 dB greater than the Raman gain in SR structure, for input pump power of 0.3 W. To achieve greater Raman gain we presented the two-ring Raman amplifier structures. Longer signal path in two-ring Raman amplifier structures gives larger Raman gain. Obtained Raman gain from 2-ring SR structure and 2-ring SR-a structure are 13.56 and 19.01 dB, respectively, for input pump power of 0.3 W.

On the other hand, passing the input pulse through the waveguide, creates dispersion and therefore signal pulse is broadened in time domain. Thus, the minimum distance between successive pulses increases and bit rate is reduced.

Optofluidic materials in SR-a structure increases the dispersion and consequently deteriorates the bit rate.

But the decline of bit rate against increasing the Raman gain is not so considerable. Thus, using improved 2-ring PhC-based Raman amplifier (2-ring SR-a) is suggesting for amplifying signal.

References

1. Rong H et al (2007) Monolithic integrated ring resonator Raman silicon laser and amplifier. Proc. SPIE 6485:1–8
2. Jalali B, Raghunathan V, Shori R (2006) Prospects of silicon Mid-IR raman lasers. IEEE J Sel Top Quantum Electron 12:1618–1627
3. Claps R et al (2004) Influence of nonlinear absorption on Raman amplification in silicon waveguides. Opt Express 12:2774–2780
4. Liu A, Rong H, Paniccia M (2004) Net optical gain in a low loss silicon-on-insulator waveguide by stimulated Raman scattering. Opt Express 12:4261–4268
5. Rukhlenko ID, Premaratne M (2010) Spectral compression and group delay of optical pulses in silicon Raman amplifiers. Opt Lett 35:3138–3140
6. Kroeger F et al (2010) Saturation of the Raman amplification by self-phase modulation in silicon nanowaveguides. Appl Phys Lett 96:241102-1–241102-3
7. Claps R et al (2005) Raman amplification and lasing in SiGewaveguides. Opt Express 13:2459–2466
8. Seidfaraji A, Ahmadi V (2012) Enhanced Raman amplification by photonic crystal based waveguide structure. ICTON 1–4
9. Seyedfaraji A, Ahmadi V (2013) Improvement of Raman amplifier bandwidth by means of slow light in photonic crystal based waveguide structure. Opt Quant Electron 45:1237–1248
10. Seyedfaraji A, Ahmadi V (2010) Enhanced Raman amplification by hybrid photonic crystals. ICTON 1–4
11. Yi-Hua H, Iwamoto S, Arakawa Y (2013) Design of slow-light grating waveguides for silicon Raman amplifier. CLEO-PR 1–2
12. Krause M, Renner H, Brinkmeyer E (2010) Silicon Raman amplifiers with ring-resonator-enhanced pump power. IEEE J Sel Top Quant 16:216–225
13. Rukhlenko ID et al (2010) Optimization of Raman amplification in silicon waveguide with finite facet reflectivities. IEEE J Sel Top Quant 16:226–233
14. Monat C et al (2010) Slow light enhanced nonlinear optics in silicon photonic crystal waveguides. IEEE J Sel Top Quantum Electron 16:344–356
15. Corcoran B (2010) Optical signal processing on a silicon chip at 640 Gb/s using slow-light. Opt Express 18:7770–7781
16. McMillan JF et al (2006) Enhanced stimulated Raman scattering in slow-light photonic crystal waveguides. Opt Lett 31:1235–1237
17. Seyedfaraji A, Ahmadi V (2013) New design of ring-based Raman amplifier using optofluidic materials. Opt Eng 59(9):097103-1–097103-6
18. Seyedfaraji A, Ahmadi V (2016) Enhanced Raman amplification by conventional and hybrid photonic crystal based ring structure. Optical Quantum Electronic 48(190):1–13
19. Bakhshi S, Moravvej-Farshi MK, Ebnali-Heidari M (2011) Proposal for enhancing the transmission efficiency of photonic crystal 60° waveguide bends by means of optofluidic infiltration. Appl Opt 50:4048–4053
20. Bakhshi S, Moravvej-Farshi MK, Ebnali-Heidari M (2012) Design of an ultracompact low-power all-optical modulator by means of dispersion engineered slow light regime in a photonic crystal Mach-Zehnder interferometer. Appl Opt 51:2687–2692

21. Dekker R et al (2007) Ultrafast nonlinear all-optical processes in silicon-on-insulator waveguides. J Phys D Appl Phys 40:R249–R271
22. Keyvaninia S et al (2008) Gain variation of Raman amplifier in silicon micro-ring coupled resonator optical waveguides. Proc SPIE 6998:699818-1–699818-8
23. Kippenberg, TJA (2004) Nonlinear optics in ultra-high-Q whispering-gallery optical microcavities. PhD thesis, California Institute of Technology
24. Lin Q, Painter OJ, Agrawal GP (2007) Nonlinear optical phenomena in silicon waveguides: modeling and applications. Opt Express 15:16604–16644
25. Zheng W et al (2009) Integration of photonic crystal polarization beam splitter and waveguide bend. Opt Express 17:8657–8668
26. Xing FF et al (2005) Optimization of bandwidth in 60-photonic crystal waveguide bends. Opt Commun 248:179–184